



**HAL**  
open science

# Inverse gas chromatography a tool to follow physicochemical modifications of pharmaceutical solids: Crystal habit and particles size surface effects

María Graciela Cares Pacheco, Rachel Calvet, Guadalupe Vaca Medina, A.  
Rouilly, Fabienne Espitalier

## ► To cite this version:

María Graciela Cares Pacheco, Rachel Calvet, Guadalupe Vaca Medina, A. Rouilly, Fabienne Espitalier. Inverse gas chromatography a tool to follow physicochemical modifications of pharmaceutical solids: Crystal habit and particles size surface effects. *International Journal of Pharmaceutics*, 2015, 494 (1), pp.113-126. 10.1016/j.ijpharm.2015.07.078 . hal-01611017

**HAL Id: hal-01611017**

**<https://hal.science/hal-01611017>**

Submitted on 5 Sep 2018

**HAL** is a multi-disciplinary open access archive for the deposit and dissemination of scientific research documents, whether they are published or not. The documents may come from teaching and research institutions in France or abroad, or from public or private research centers.

L'archive ouverte pluridisciplinaire **HAL**, est destinée au dépôt et à la diffusion de documents scientifiques de niveau recherche, publiés ou non, émanant des établissements d'enseignement et de recherche français ou étrangers, des laboratoires publics ou privés.

# Inverse gas chromatography a tool to follow physicochemical modifications of pharmaceutical solids: Crystal habit and particles size surface effects

M.G. Cares-Pacheco<sup>a,\*</sup>, R. Calvet<sup>a</sup>, G. Vaca-Medina<sup>b,c</sup>, A. Rouilly<sup>b,c</sup>, F. Espitalier<sup>a</sup>

<sup>a</sup> Université de Toulouse; Mines Albi, UMR CNRS 5302, Centre RAPSODEE; Campus Jarlard, F-81013 Albi cedex 09, France

<sup>b</sup> Université de Toulouse; INP-ENSIACET, LCA, 310130 Toulouse, France

<sup>c</sup> INRA; UMR 1010 CAI, 310130 Toulouse, France

## ABSTRACT

Powders are complex systems and so pharmaceutical solids are not the exception. Nowadays, pharmaceutical ingredients must comply with well-defined draconian specifications imposing narrow particle size range, control on the mean particle size, crystalline structure, crystal habits aspect and surface properties of powders, among others. The different facets, physical forms, defects and/or impurities of the solid will alter its interaction properties. A powerful way of studying surface properties is based on the adsorption of an organic or water vapor on a powder. Inverse gas chromatography (IGC) appears as a useful method to characterize the surface properties of divided solids.

The aim of this work is to study the sensitivity of IGC, in Henry's domain, in order to detect the impact of size and morphology in surface energy of two crystalline forms of an excipient, D-mannitol. Surface energy analyses using IGC have shown that the  $\alpha$  form is the most energetically active form. To study size and shape influence on polymorphism, pure  $\alpha$  and  $\beta$  mannitol samples were cryomilled (CM) and/or spray dried (SD). All forms showed an increase of the surface energy after treatment, with a higher influence for  $\beta$  samples ( $\gamma_s^d$  of 40–62  $\text{mJ m}^{-2}$ ) than for  $\alpha$  mannitol samples ( $\gamma_s^d$  of 75–86  $\text{mJ m}^{-2}$ ). Surface heterogeneity analysis in Henry's domain showed a more heterogeneous  $\beta$ -CM sample (62–52  $\text{mJ m}^{-2}$ ). Moreover, despite its spherical shape and quite homogeneous size distribution,  $\beta$ -SD mannitol samples showed a slightly heterogeneous surface (57–52  $\text{mJ m}^{-2}$ ) also higher than the recrystallized  $\beta$  pure sample ( $\sim 40 \text{ mJ m}^{-2}$ ).

### Keywords:

D-mannitol

Polymorphism

Surface energy

Inverse gas chromatography

Spray drying

Cryomilling

## 1. Introduction

Pharmaceutical solids must comply with well-defined specifications in terms of bioavailability, solubility, toxicity and stability. Nowadays, the requirements are more and more draconian, imposing narrow particle size range, control on the mean particle size, crystalline structure, crystal habits aspect and surface properties of powders, among others. A large set of operations is developed to answer these requirements. The processes for producing fine powders (around micrometer) are varied as melt quenching, grinding, freeze-drying, spray drying, crystallization, antisolvent precipitation, milling, and supercritical fluids. Depending upon the nature of the active pharmaceutical ingredients (APIs), it is known that the preparation method influences the

physical stability and crystallization behavior. The impact of these processes on solid phase transformations may lead to the formation of a metastable or an amorphous form, or a mixtures of various crystalline forms including other hydrates (or solvates). These changes are desired for certain stages of the formulation or for some use properties of the API, but sometimes can also have undesirable effects on the solid.

Inverse gas chromatography (IGC) appears as a tool to study the changes on surface properties in order to highlight process influences to assess drug delivery systems performance. Mechanical operations are the most studied processes to determine pharmaceutical solids surface's behavior. Most authors described an increase of the dispersive component of the solid surface energy,  $\gamma_s^d$ , after mechanical grinding (Table 1). This increase is generally attributed to the exposure of specific crystal facets that present different chemical groups, the formation of higher energy zones such as crystal defects, dislocations and/or to solids state transformations (Chamarthy et Pinal, 2008; Feeley et al., 2002;

\* Corresponding author.

E-mail address: [gcares@mines-albi.fr](mailto:gcares@mines-albi.fr) (M.G. Cares-Pacheco).

## Nomenclature

$a_s$ (m <sup>2</sup> /g)	Specific surface area of the solid
$d$ (n,0.5) (μm)	Number median diameter
$D$ [v,0.5] (μm)	Median volume diameter
$\Delta g_{ads}$ (J/mol)	Molar free energy variation for an isothermal adsorption of probe molecules
$m$ (g)	Sample mass
$n$ (mol)	Desorbed mole number
$n_{ads}$ (μmol/g)	Adsorbed mole number per gram of solid
$n_m$ (mol)	Monolayer capacity or number of adsorbed moles corresponding to a monolayer
$P$ (Pa)	Vapor pressure or partial pressure
$P_{sat}$ (Pa)	Saturation vapor pressure
$T$ (K)	Temperature
$T_c$ (K)	Column temperature
$t_N$ (min)	Net retention time
$V_N$ (cm <sup>3</sup> )	Net retention volume
$W_{adh}$ (J/m <sup>2</sup> )	Work of adhesion when adsorption occurs
$n/n_m$ (-)	Surface coverage

## Greek symbols

$\gamma_l^d$ (J/m <sup>2</sup> or N/m)	Liquid surface energy (or surface tension)
$\gamma_s^d$ (J/m <sup>2</sup> or N/m)	Dispersive component of solid surface energy
$\gamma_s$ (J/m <sup>2</sup> or N/m)	Total surface energy of a solid
$\gamma_s^{sp}$ (J/m <sup>2</sup> or N/m)	Specific component of solid surface energy
$\theta_s$ (-)	Surface coverage

**Table 1**

An overview of the influence of particles size reduction over the surface properties of pharmaceutical ingredients by IGC.

Pharmaceutical solid	$\gamma_s^d$	Reference
Acetaminophen	↑	Trowbridge et al. (1998) Heng et al. (2006)
Cefditoren pivoxil	↓	Ohta and Buckton (2004)
DL-propranolol hydrochloride	↑	York et al. (1998)
Felodipine	↑	Chamarthy and Pinal (2008)
		Chamarthy and Pinal (2008)
Griseofulvine	↑	Feng et al. (2008)
	↓	Otte and Carvajal (2011) Otte et al. (2012)
Ibipinabant	↑	Gamble et al. (2012)
Indomethacin	↑	Planinsek et al. (2010) Lim et al. (2013)
		Ahfat et al. (2000) Feeley et al. (2002)
Lactose	↑	Newell and Buckton (2004) Thielmann et al. (2007) Shariare et al. (2011) Brum and Burnett (2011) Jones et al. (2012)
Mannitol	↑	Ho et al. (2012)
Salbutamol sulfate	↑	Ticehurst et al. (1994) Feeley et al. (1998)
Salmeterol Xinofoate	↑	Tong et al. (2001, 2006) Das et al. (2009)
Sucrose	↑	Surana et al. (2003) Hasegawa et al. (2009) Luner et al. (2012)
Succinic acid	↑	Luner et al. (2012)

Feng et al., 2008; Heng et al., 2006; Ho et al., 2012; Newell and Buckton, 2004).

### 1.1. Surface energy, particles size and surface chemistry

Due to the anisotropic nature of powders, the exhibition of new crystal faces under milling can change the acidic/basic character of the solid depending on the functional groups present in the exposed facets. Heng et al. (2006) highlighted the anisotropic nature of form I paracetamol crystals. The confrontation of sessile drop and IGC, allowed them to conclude that grinding leads to a fragmentation of the facet (010), which possesses the weakest attachment energy and exhibits the large  $\gamma_s^d$ . Thus, after milling the  $\gamma_s^d$  of the samples increased, showing a more hydrophobic surface, with decreasing particle size.

York et al. (1998) were interested in the milling of DL-propranolol hydrochloride. The evolution of  $\gamma_s^d$  showed to depend on the particles size. During milling the surface becomes increasingly more energetic ( $\gamma_s^d$  from 45 to 61 mJ/m<sup>2</sup> for particles 75–16.5 μm) until reached a plateau followed by a small fall in  $\gamma_s^d$  for the finest powder (<10 μm). The authors concluded that the increases in  $\gamma_s^d$ , and in  $\Delta g_{ads}$  using CH<sub>2</sub>Cl<sub>2</sub> as probe molecule, are due to a fragmentation releasing the dominant crystal face, which posses the lowest attachment energy and is rich in naphthalene groups. Attrition might become significant as milling intensity increase releasing faces having OH groups, naphthalene and Cl<sup>-</sup> ions.

Trowbridge et al. (1998) highlighted that acetaminophen size reduction from 30 to 10 μm led to an increase of  $\gamma_s^d$  from 50.9 to 61.3 mJ/m<sup>2</sup> and to an increase of  $\Delta g_{ads}$  from 327 to 506 J/mol, using chloroform as probe molecule. Milling also increases the hydrophobic and basic character of acetaminophen surface. This results

are in agreement with those obtained by molecular modeling which established that milling leads to the exposure of the crystal facet (010) which contain an hydrophobic methyl group, a benzene ring and a carboxyl group, both basic.

Ohta and Buckton (2004) studied surface energetic changes of cefditoren pivoxil, a cephalosporin antibiotic, as consequence of milling. After grinding in a vibration mill, the authors found a decrease in the  $\gamma_s^d$  according to the grinding time, from 52.3 mJ/m<sup>2</sup> before milling to 45.8 mJ/m<sup>2</sup> after 30 min of grinding with a decrease in solid crystallinity. In addition, the authors have shown a decrease in the solid acidic character with an increased on its basicity. These effects are attributed to the exposure of carbonyl groups, which have an electron donating nature.

Luner et al. (2012) studied by IGC the impact of high shear wet milling (HSWM) and dry milling (DM) on the surface properties of two pharmaceutical compounds, succinic acid and sucrose. Physicochemical characterization of both samples showed that bulk properties were unaffected by wet and dry milling while surface properties analyses showed an increase of solids dispersive surface energy after DM and HSWM. Succinic acid samples,  $\gamma_s^d$  = 35 mJ/m<sup>2</sup>, exhibit minor differences between dry milled and wet milled samples, 40 ± 2 mJ/m<sup>2</sup>, attributed to minimal impact of cleavage and the exposure of crystal facets with similar atomic surface arrangements. For HSWM sucrose, the polarity of the solvents used during wet milling influenced  $\gamma_s^d$  of the milled samples from 55 to 71 to 91 mJ/m<sup>2</sup>, for hexane, methyl tertiary butyl ether and ethanol respectively while dry milled samples exhibit a  $\gamma_s^d$  of 44 mJ/m<sup>2</sup>. Differences between dry and wet milling processes were attributed to the attrition mechanism in presence of solvent.

Reducing particle size may also be necessary for the API to reach the target organ, particularly when the drug administration is by

inhalation. Nowadays, dry powder inhalers (DPIs) are of great interest thanks to the absence of propellant and the stability of the formulation as a result of the dry state. A successful drug delivery will depend on the interaction between the powder formulation and the device performance. During inhalation, the API detaching from the carrier by the energy of the inspired airflow that overcomes the adhesion forces between the API and the carrier. Over the past few years, lactose has been considered as the excipient of choice in several solid oral dosage forms and so many studies have been carried on lactose, most of them based on the study of its physical–chemical properties as function of the manufacturing process (Pilcer et al., 2012). Thus, why lactose is also the most studied organic solid by IGC. Feeley et al. (2002) and Shariare et al. (2011) studied the influence of milling on the surface properties of lactose. IGC analyses showed a low sensitivity of  $\gamma_s^d$  to milling. However, the study of basic and amphoteric probes showed changes of the hydroxyl groups presented in lactose surface. Shariare et al. (2011) also highlighted that the acidic or basic character of the powder seems to be related to the size of starting particles. For sample, the micronization of larger particles, 50–100  $\mu\text{m}$ , results in an increase of the specific component of solid surface energy,  $\gamma_s^{\text{SP}}$ , measured with THF (basic probe). While the micronization of finer particles, <20  $\mu\text{m}$ , leads to an increase of  $\gamma_s^{\text{SP}}$  using amphoteric probes molecules such as acetone.

## 1.2. Surface energy and crystalline solid state

Tong et al. (2001, 2006) studied the influence of solid–solid interactions on the aerosol performance of salmeterol xinafoate (SX) polymorphs and lactose carrier by IGC. SX is a highly selective bronchodilator, known to exist in two crystalline forms. Three active batches of SX were generated: the two polymorphs, SXI and SXII, crystallized using solution enhanced dispersion by supercritical fluids from methanol solution (SEDS) and a form called MSXI generated by the micronisation of the SXI form. First of all, dispersive surface energy analysis by IGC exhibits a more active MSXI sample ( $\gamma_{\text{SXI}}^d \sim 33 \text{ mJ/m}^2$ ,  $\gamma_{\text{SXII}}^d \sim 29 \text{ mJ/m}^2$  and  $\gamma_{\text{MSXI}}^d \sim 39 \text{ mJ/m}^2$ ). IGC was also applied to calculate the cohesion between SX samples and the adhesion between the samples of SX and lactose. The study of the strength drug–drug cohesion and drug–carrier adhesion suggests that the active particles of SX bond more strongly to the carrier particles of lactose than to those of their own species, except for SXII–lactose: SXI–SXI (190.7 MPa), SXII–SXII (67.3 MPa), MSX–MSX (245.0 MPa), SXI–lactose (212.6 MPa) SXII–lactose (47.5 MPa), MSXI–lactose (278.1 MPa). The use of lactose as a carrier improves aerosol performance about 25% for the batch SXI and 140% for the batch MSXI.

Traini et al. (2008) studied by IGC the lactose–salbutamol sulfate interactions in DPI formulations. The aim was to investigate lactose pseudo-polymorphs,  $\alpha$ -anhydrous,  $\alpha$ -monohydrate and  $\beta$ -anhydrous, in terms of carrier functionality. In this work,  $\alpha$ -monohydrate form exhibits best aerosol performance, indicating that carrier surface chemistry plays a dominating role in DPIs. The authors also highlighted an inverse relationship between surface energy and aerosol efficiency.

More recently studies has been carried out in order to provide a substitute for  $\alpha$ -lactose monohydrate as carrier in DPI formulations. Indeed, lactose possesses several drawbacks due to its bovine origin, its incompatibility with amino groups like peptides and proteins and its tendency to become amorphous after mechanical treatment. Nowadays, mannitol appears to be an adequate substitute for lactose because it does not carry reducing groups that may cause chemical interaction with proteins and is highly crystalline even upon spray drying (Maas et al., 2011).

Surface energy analysis of D-mannitol has been focused on the stable  $\beta$  form. IGC has highlighted its acidic nature, attributed to the high density of hydroxyl groups at mannitol surface (Saxena et al., 2007). More recently research were focused on the effect of milling and/or surface energy heterogeneity of the stable  $\beta$  form (Ho et al., 2010, 2012). Our previous research work, Cares et al. (2014), was focused on the study of D-mannitol polymorphs. D-mannitol pure polymorphs exhibit a more active and highly heterogeneous  $\alpha$  form (74.9 to 45.5  $\text{mJ/m}^2$ ) with a less active and quite homogeneous stable  $\beta$  mannitol ( $\sim 40$ – $38 \text{ mJ/m}^2$ ), which also behave similarly to the instable  $\delta$  form. Mannitol particles, generated by SD, have been used commercially in bronchial provocation test (Aridol). Tang et al. (2009) studied the impact of different generation processes in particles to improve aerosol performance. Three powder samples were prepared: by confined liquid impinging jets (CLJJs) followed by jet milling (JM), SD and JM. These processes generated quite different powder samples, needle-shape for CLJJs samples, spherical for SD samples and orthorhombique for the JM samples. Dispersive surface energy analysis by IGC exhibits a more active CLJJs sample attributed to the presence of  $\alpha$  mannitol ( $\gamma_{\text{CLJJs}}^d \sim 85 \text{ mJ/m}^2$ ,  $\gamma_{\text{SD}}^d \sim 60 \text{ mJ/m}^2$  and  $\gamma_{\text{JM}}^d \sim 48 \text{ mJ/m}^2$ ). Particles shape showed to be an important contributor to the aerosol performance of mannitol powders as it affects the surface energy and particles dynamics.

Yamauchi et al. (2011) studied physicochemical differences with emphasis on the surface properties, by IGC and DVS, of niclosamide and naproxen sodium and their respective anhydrate and dehydrated hydrated forms. The naproxen sodium anhydrate form showed a higher  $\gamma_s^d$  and higher rate of moisture sorption than the dehydrated hydrated form, whereas the opposite was observed for niclosamide.

## 1.3. Surface energy, defects and amorphization

Many APIs are poorly soluble in water, which limits their bioavailability. Their rate of dissolution may improve by using an amorphous phase of the API. Indomethacin (IDMC) is a good example. IDMC is an antipyretic and anti-inflammatory drug used in many pharmaceutical formulations, it has four polymorphs and an amorphous. According to the grinding temperature, below or higher than its glass transition temperature ( $T_g$ ), and grinding intensity the most stable form at ambient conditions,  $\gamma$ -IDMC, can transform to the metastable  $\alpha$  form or lead to an amorphous state (Crowley and Zografi, 2002; Desprez and Descamps, 2006). As IDMC is highly insoluble in water (0.02  $\text{mg/mL}$ ), the bioavailability of the product and its absorption by the gastrointestinal tract can be improved by using an amorphous form of the drug (Imaizumi et al., 1980). Planinsek et al. (2010) studied the crystalline fraction that transforms into amorphous forms upon intensive milling. IGC was used to detect surface changes caused by milling crystalline  $\gamma$ -IDMC while DSC was used to determine the mass (or equivalent volume) fraction of the samples transformed. The authors determined that the dispersive energy of the stable  $\gamma$ -IDMC was 32.2  $\text{mJ/m}^2$  and that of the amorphous, generated in a ball mill for 120 min, of 43.3  $\text{mJ/m}^2$ . Studies on the influence of milling time, allows the authors to illustrate the sensitivity of the IGC-ID to detect crystal surface defects as high-energy sites ( $\gamma_{30\text{min}}^d = \gamma_{60\text{min}}^d = \gamma_{\text{amorphe}}^d$ ). By comparing time evolution of the amorphous fraction of the surface by IGC and volume by DSC the authors showed that surface transforms at higher rate (an order of magnitude) than the bulk phase. IGC seems to be a powerful tool to quantify amorphous rate and to locate it by the confrontation with bulk (or volume) measurement techniques (Brum and Burnett, 2011).

The development of cost-efficient technologies for the generation of drug powders with desired physicochemical properties is still a challenge for pharmaceutical companies. To actually define a successful protocol it seems necessary to study surface energy as a function of polymorphism, surface chemistry of the exposed facets, particles size and shape (crystal habits). Nevertheless, as can be depicted, it is quite difficult to actually distinguish each effect influence. The objective of this work is to quantify the effect of size and crystal habits in surface energy of an API, D-mannitol.

To study particles size and shape influence on surface energetics of D-mannitol polymorphs two techniques are used: spray drying and/or cryomilling. As mannitol is known to be highly crystalline even during milling or spray drying, size reduction processes used in this work were established in ways that polymorphs solids samples do not undergo any phase transformation. IGC at infinite dilution (IGC-ID) is used to study solid surface anisotropy at low surface coverage, while DVS will be used to have a more global view of the interaction potential. The dual aim of this work is to highlight the impact of size and crystal habits on the adsorption behavior of different anhydrous forms of D-mannitol and to compare the surface energy determination techniques used pointing out their relevance considering the physical sense of the measure.

## 2. Materials and methods

### 2.1. Materials

D-mannitol was generously provided by Roquette (France). The batch, Pearlitol 160C, is composed of 99% of  $\beta$  mannitol mass percentage and only 1% of sorbitol. High purity deionized water (18 M $\Omega$  cm) was obtained from a laboratory purification system. The non-polar probes octane, nonane and decane were purchased from Sigma, assay >99%.

### 2.2. Generation and formulation protocols

#### 2.2.1. Crystallization

Pure  $\beta$  and  $\alpha$  forms were generated by antisolvent precipitation (acetone) and by seeding and fast cooling respectively as described previously in [Cares et al. \(2014\)](#).

#### 2.2.2. Spray drying (SD)

The experiments were performed using a laboratory mini spray dryer Büchi B-290 equipped with a two-fluid nozzle of 0.5 mm diameter. The flow rate of the aqueous mannitol solutions, 10 g/L, is set at 6 mL/min and the atomizing air rate at 600 NL/h. Air inlet temperature is set to 120 °C while outlet temperature was measured by a temperature sensor in the air exit point, noted 87 °C. To recover the powder the aspiration is set to 35 m<sup>3</sup>/h (maximum level). Samples were stored at room temperature under vacuum in glass desiccators containing silica gel (relative humidity of 6%).

#### 2.2.3. Cryomilling (CM)

A Retsch cryogenic impact mill was used for milling. Samples of around 500 mg were placed in stainless steel grinding jars of 5 mL containing one stainless steel grinding ball of 5 mm diameter. The samples were milled for 4 cycles in total, each consisting of a 10 min grinding time at 25 Hz followed by intervals of 0.5 min at 5 Hz. The samples were continually cooled with liquid nitrogen before and during the grinding process.

### 2.3. Particles physicochemical characterization

#### 2.3.1. Chemical purity

The chemical purity of each sample was checked by HPLC using a Hi-Plex Ca ligand exchange column coupled with a refractive

index detector (analysis conditions: mobile phase HPLC grade water, flow rate 0.3 mL min<sup>-1</sup>, column temperature 45 °C).

#### 2.3.2. Polymorphs finger prints

The mannitol powder samples were analyzed using different techniques to confirm the identity of the different polymorphs. X-ray powder diffraction patterns (XRPD) were obtained using a PANalytical X'Pert Pro MPD diffractometer (set-up Bragg-Brentano). Diffraction data is acquired by exposing the powders samples to Cu-K $\alpha$  radiation at a voltage of 45 kV and to a current of 40 mA. The data were collected over a range of 8–50° 2 $\theta$  at step size of 0.03°. Quality diffraction patterns were obtained in a relatively short exposure time (20 min). Data analysis is done with the X'Pert Data Collector software while phase identification is made with PANalytical High Score More software and databases "ICDD Powder Diffraction File 2" and "Crystallography Open Database".

FT-Raman spectra were recorded with an atomic force microscope equipped with a confocal Raman imaging upgrade, Alpha 300 from WITec. A magnification of 50 $\times$  and an excitation source of Nd:YAG (532 nm) were used. The Raman data were acquired using WITec Project Plus software that has a 16 bits resolution and a sampling rate of 250 Hz.

Thermal analysis was performed with a DSC Q200 from TA Instrument. Samples amount of about 3–5 mg are placed in non-hermetic aluminum panels, in the temperature range of 20–200 °C at a heating rate of 5 °C/min under nitrogen atmosphere. Nitrogen flow was adjusted at 50 mL/min. All data measurements are averages of at least 3 measures on 3 different samples. Heat of fusion values were determined using a sigmoid baseline with a standard deviation of less than 0.5% (6 measures average).

#### 2.3.3. Size and particle shape analysis

Particle shape analyses were examined using a XL30 SEM, scanning electron microscopy, with a field emission gun (FEG) operating at 15 or 20 kV. Samples were placed onto doubled-sided adhesive and coated with Platinum for 4 min using an auto sputter coater SC7640 under argon gas purge.

The particle size analysis was performed by image analysis using an optical banc PharmaVision System PVS 830 from Malvern Instruments. To separate the particles, a pressure of 6 bar was set (SPD 1300). The number of particles to be analyzed was set at 70,000. Two objectives were used "zoom 3" which can analyze a particle size range between 310 and 7.5  $\mu$ m, with a resolution of 7  $\mu$ m and "zoom 5" which allows to analyze a particle range between 100 and 1.7  $\mu$ m with a resolution of 3  $\mu$ m.

#### 2.3.4. Surface analysis techniques

Specific surface area and surface energy analyses of D-mannitol polymorphs were carried out using an IGC-Surface Energy Analyser (IGC-SEA) from SMS. Each powder sample was packed into pre-silanised columns of 300 mm length and 4 mm internal diameter, plugged with silanised glass wool. Prior to analysis, each column was conditioned at 50 °C for 2 h at 0% RH. Helium was used as a carrier gas at 10 sccm and the column temperature was fixed at 30 °C during the analysis, all experiences were undertaken in identical conditions. The retention times of probe molecules and methane were determined using a flame ionization detector (FID). Dead volume was determined by methane injections and dispersive surface energy determination by a homologous series of *n*-alkanes (*n*-decane, *n*-nonane and *n*-octane). Dispersive surface energy profiles were calculated using Cirrus Plus software (version 1.2.3.2 SMS, London) following Dorris-Gray approach. The corresponding surface coverage,  $\theta_s$ , at each injection concentration is the ratio between the desorbed

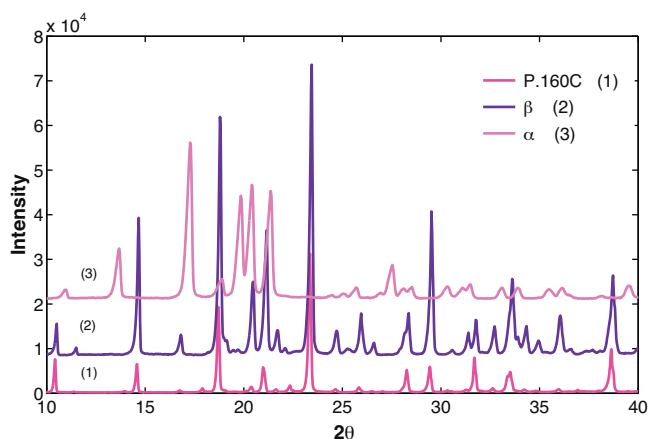


**Fig. 1.** X-ray patterns of depart samples,  $\alpha$  and  $\beta$  mannitol and the commercial form Pearlitol 160C.

amount,  $n$ , determined from peak area and the monolayer capacity of the solid,  $n_m$  ( $\theta_s = n/n_m$ ). In our experiments,  $n_m$  was determined from the specific surface area value obtained by IGC–SEA using  $n$ -nonane as probe molecule. Full details of the experimental procedure and analysis by IGC have been published previously (Cares et al., 2014).

### 3. Results

#### 3.1. *D*-mannitol depart samples

##### 3.1.1. Powder crystallinity and purity

XPRD patterns of the commercial form P160C and the pure forms  $\beta$  and  $\alpha$  mannitol are shown in Fig. 1. As it is depicted from the figure,  $\alpha$  mannitol has characteristic reflection peaks at  $2\theta$  positions of 13.7°, 17.3° and 19.9° and 21.4° while for  $\beta$  mannitol are located at 14.7°, 18.8°, 23.6° and 29.5°. No differences in the characteristic reflection peaks between the commercial powder

**Table 2**

Summary of physical solid-state characterization obtained by DSC.

	P160C	$\beta$ -form	$\alpha$ -form
Heat of fusion ( $\text{J g}^{-1}$ )	300.2	304.5	294.4
	0.4	–	–
Melting point (onset) ( $^{\circ}\text{C}$ )	165.6	166.7	165.3
	81.4	–	–

Pearlitol 160C and the  $\beta$  pure form were found, the differences between patterns peaks intensity can be attributed to morphology differences between both samples. Indeed, sorbitol presences in the commercial powder P.160C is not detected by XPRD but is detected by DSC (Table 2). As shown in Fig. 2, the first endothermic peak at 81.4  $^{\circ}\text{C}$ , is consistent with the melting point of  $\alpha$ -sorbitol (Nezzal et al., 2009) which decreases both heat of fusion and melting point of  $\beta$  polymorph.

It should be noted that the detection of small quantities is complex and may depend on the location of sorbitol within the powder, near to the surface or within the bulk of the crystals.

#### 3.1.2. Particles size and habit

As described in our previous work, the commercial sample Pearlitol 160C (P160C) is composed by irregular sticks with a median volume diameter  $D[v, 0.5]$  of 64  $\mu\text{m}$  and a  $D[v, 0.9]$  of 250  $\mu\text{m}$  (Fig. 3a). The  $\beta$  form generated by antisolvent precipitation is formed by better-defined sticks with smoother surfaces (Fig. 3b), and it has a  $D[v, 0.5]$  of 26.7  $\mu\text{m}$  and a  $D[v, 0.9]$  of 81.7  $\mu\text{m}$ . It seems that for both samples, the smaller particles get stuck on the surface of the largest ones.

The  $\alpha$  form is the finest one with needle-shape morphology and a  $D[v, 0.5]$  of 25.3  $\mu\text{m}$  and a  $D[v, 0.9]$  of 42.4  $\mu\text{m}$  (Fig. 3c). It should be notice that particles size analysis using PVS 830 seems to be not well adapted for the  $\alpha$  form analysis. In fact SEM analysis showed a narrower size distribution. It is possible that PVS 830 characterizes particles agglomerations due to higher cohesion forces between these particles.

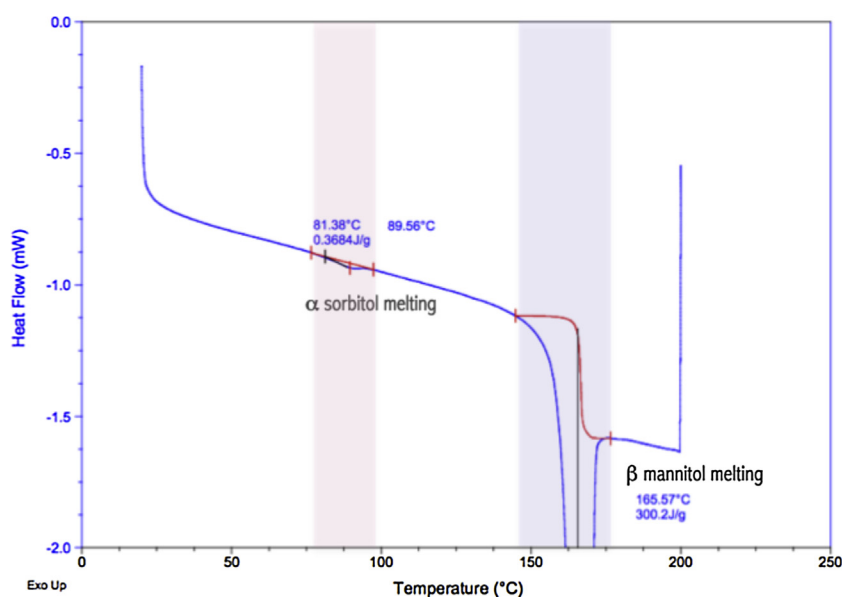


**Fig. 2.** DSC profile of the commercial powder Pearlitol 160C, heating rate of 5  $^{\circ}\text{C}/\text{min}$ .

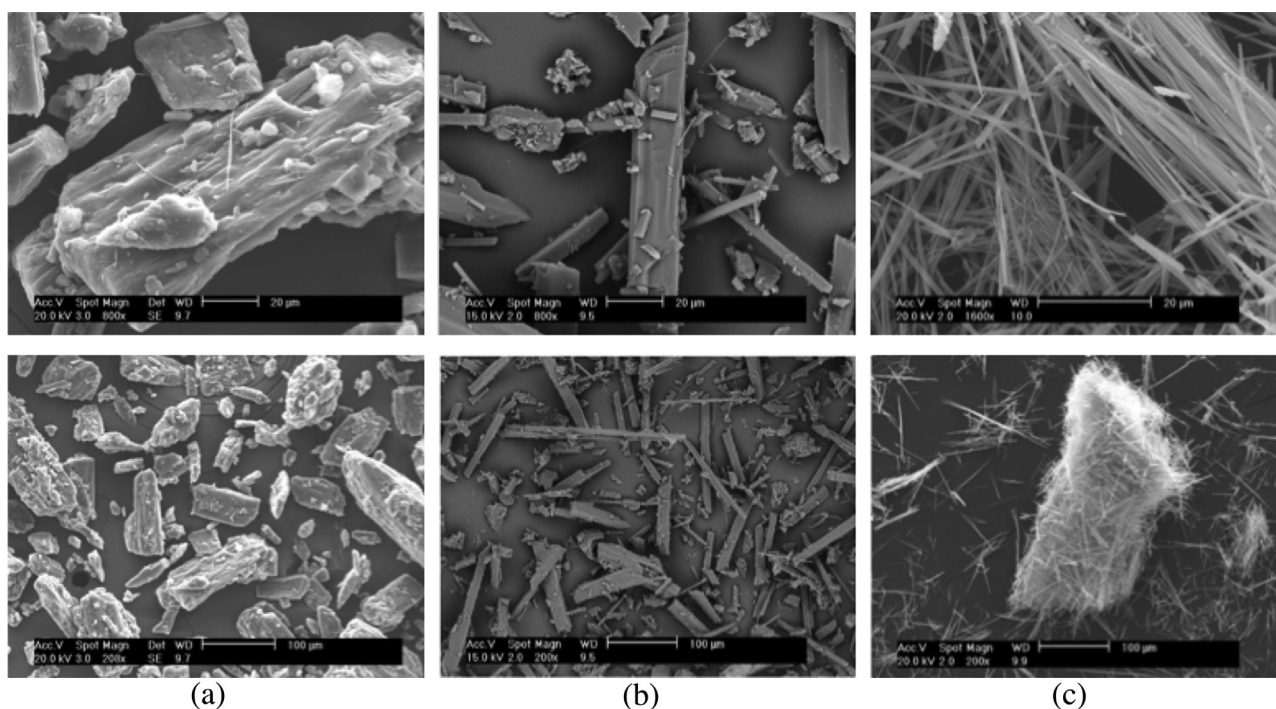


Fig. 3. SEM micrographs of (a) commercial powder Pearlitol160C, (b) pure  $\beta$  mannitol and (c) pure  $\alpha$  mannitol.

### 3.2. Spray dried samples (SD)

Two samples were generated by spray drying two different  $\beta$  mannitol batches. The first one correspond to a pure  $\beta$  mannitol obtained by antisolvent crystallization and the second batch to the commercial powder Pearlitol 160C. The abbreviations  $\beta$ -SD and P160C-SD are used in this manuscript to differentiate them.

#### 3.2.1. Powder crystallinity and purity

XPRD patterns revealed that the two SD samples are composed of the stable  $\beta$  form (Fig. 4). The small peak present at  $17.3^\circ$  can be attributed to the presence, in really small quantities, of  $\alpha$  mannitol. Nevertheless not other characteristic peaks from the  $\alpha$  form were found in the patterns. Moreover, DSC and Raman spectroscopy analysis do not corroborate the presence of  $\alpha$  mannitol in the samples. The differences between the patterns peaks intensity can be attributed to the morphology differences.

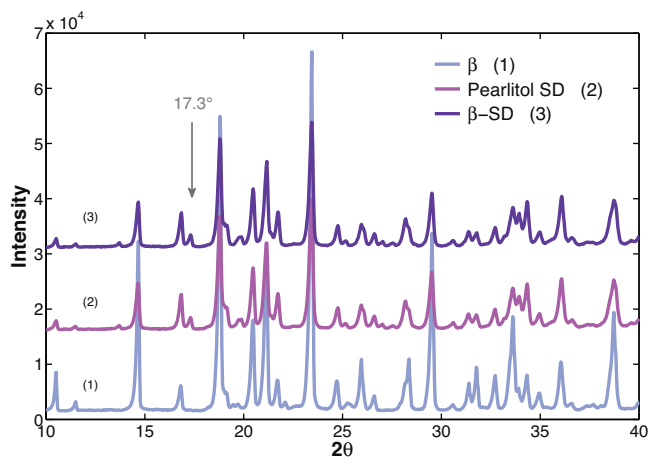


Fig. 4. X-ray patterns of  $\beta$  mannitol samples before and after spray drying.

Some protocols to spray dry D-mannitol aqueous solutions can be found in the literature, differentiating in polymorphs generation. For example, Lee et al. (2011) obtained only the stable  $\beta$  form after SD while Maas et al. (2011) showed that outlet temperatures at/below  $90^\circ\text{C}$  generated mainly  $\beta$  mannitol and small amounts of  $\alpha$  mannitol (around 5%). Outlet temperatures up to  $140^\circ\text{C}$  increased  $\alpha$  mannitol concentration within the samples (between 5 and 15%). Nevertheless, in our experiences, with an outlet temperature of  $87^\circ\text{C}$ , DSC and Raman spectroscopy analysis do not detected the presence of the  $\alpha$  form in the SD samples.

#### 3.2.2. Particles size and habit by scanning electron microscopy (SEM)

Image analysis obtained with PVS 830 cannot be used for the analysis of spray dried samples. In fact the most powerful camera lens "zoom 5" does not measure particles smaller than  $3\ \mu\text{m}$ , which seems to be a quite important population according to SEM analysis. In addition, the dispersion protocol used with the SPD 1300 does not seem to actually disperse the particles. Finally, crystal habits and size analysis has been exploited by SEM.

From a microscopic point of view ( $10\text{--}20\ \mu\text{m}$ ), the powders obtained after spray drying are homogeneous in size and morphology. SEM micrographs show quite spherical particles with diameters between  $300\ \text{nm}$  and  $10\ \mu\text{m}$  and a "quite" smooth surface (Figs. 5 and 6). These values are smaller than those obtained by Maas et al. (2011) which despite the observed differences in particle formation, the particles size distributions obtained at different outlet temperatures ( $60, 90$  and  $120^\circ\text{C}$ ) are very closed, with a mean diameter of  $13\ \mu\text{m}$ . The authors also highlighted that the spray drying of mannitol at different outlet temperatures modifies particle surface topography. In their case drying at  $60^\circ\text{C}$  leads to the formation of acicular crystal with a smooth particle surface. In contrast, at higher temperatures, the droplets evaporate much faster and do not recrystallize immediately because of the low nucleation rate at this temperature. Even if there is expected that water evaporate prior crystallization, no difference in particle size were obtained. Thus, the authors assumed that the nucleation and crystal growth also occurs in a

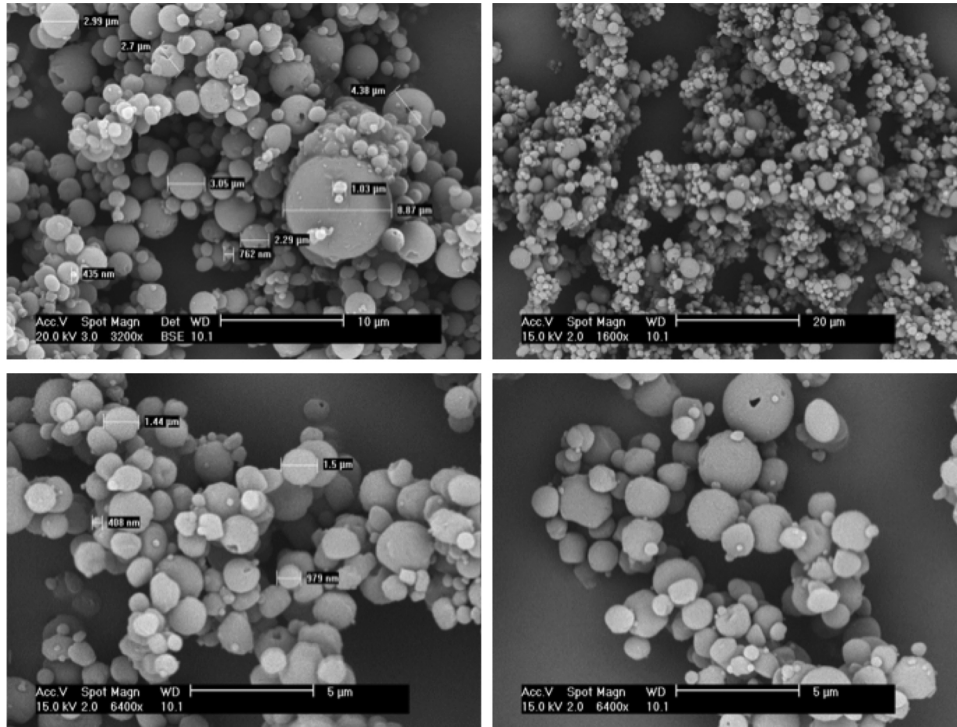


Fig. 5. SEM micrographs of pure  $\beta$  mannitol sample after spray drying.

rather early drying stage due to the high dynamic in the spray dryer and the presence of crystalline seeds that may trigger earliest crystallization. In fact, since the crystals grow larger in higher temperatures and because of the fast solvent evaporation, the forming shell becomes quickly very rigid and the openings of the

hollow particles can be seen. In our case, with an outlet temperature of 87 °C, some of the particles exhibit a rough surface and some other showed to be hollow with a well visible orifice in their shell (Figs. 5 and 6). SEM analyses were limited due to samples degradation for a magnification higher than 6400 $\times$ .

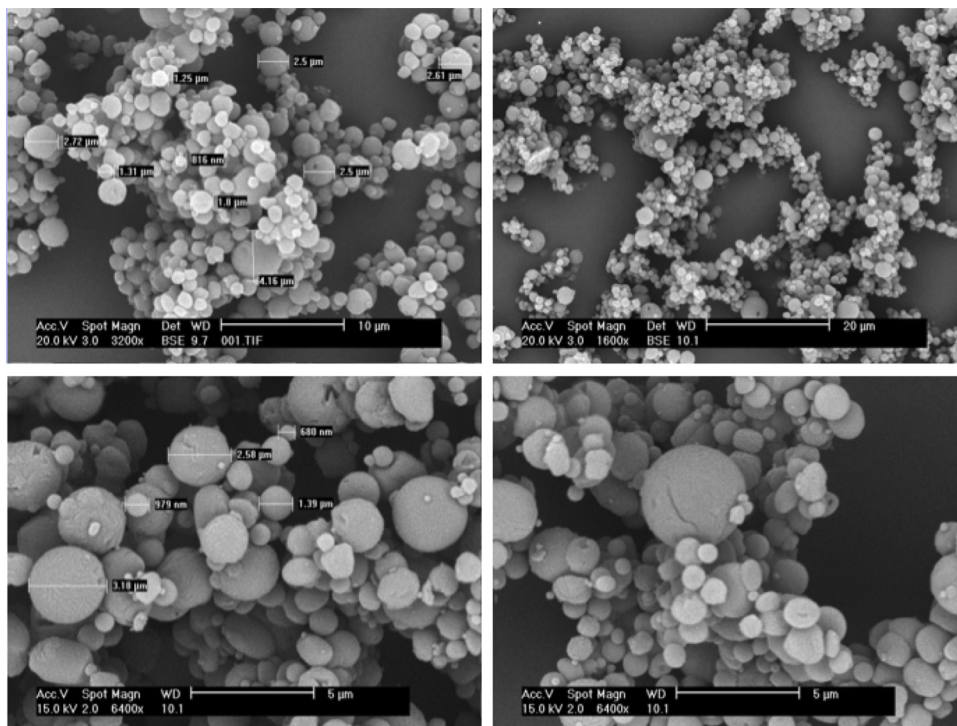


Fig. 6. SEM micrographs of commercial powder P.160C after spray drying.

**Table 3**

Specific surface areas and dispersive surface energies of different D-mannitol samples. The "X" represents the analysis that can not be done (technique limits) while "-" represents the ones that have not being done.

D-mannitol	$a_s$ ( $\text{m}^2 \text{g}^{-1}$ )		DVS	$\gamma_s^d$ ( $\text{mJ m}^{-2}$ )			
	ASAP-Ar	IGC-C <sub>9</sub>		IGC			
				$\theta_s = 0.04\%$	$\theta_s = 0.1\%$	$\theta_s = 1\%$	$\theta_s = 8\%$
P160C	0.4	0.4	X	70.7	69.1	58.0	44.9
$\alpha$	8.4	8.5	51	74.9	75.0	72.1	45.5
$\beta$	2.8	0.4	X	40.9	40.9	39.4	38.2
P160C-SD	3.4	4.0	40	62.6	62.3	55.4	X
$\beta$ -SD	2.9	4.4	41	57.2	57.3	51.7	X
$\alpha$ -CM	-	11.9	-	85.6	81.7	70.7	X
$\beta$ -CM	3.6	3.3	47	61.9	62.0	52.4	X

Finally, no differences in size and particles shape were found between  $\beta$ -SD (Fig. 5) and P.160C-SD (Fig. 6) samples.

### 3.2.3. Surface energy analysis

After spray drying  $\beta$ -SD and P160C-SD presented an increment of their specific surface area and so an increase of the vapor probes adsorbed amount (Table 3) allowing DVS analysis. Thus, both SD samples, exhibit a similar adsorption behavior with a type II isotherm (Fig. 7). Surface energy values obtained by DVS were calculated taking into account contact angle values obtained by capillary rise (Cares et al., 2014). The error associated to the measure is  $1 \text{ mJ m}^{-2}$ .

The  $\gamma_s^d$  values obtained by DVS of  $\beta$ -SD and P160C-SD samples are similar to those obtained by IGC for the  $\beta$  pure form (Table 3).

IGC-ID analyses show that  $\beta$ -SD and P160C-SD samples have similar adsorption behavior (Table 3). Moreover,  $\gamma_s^d$  values of SD

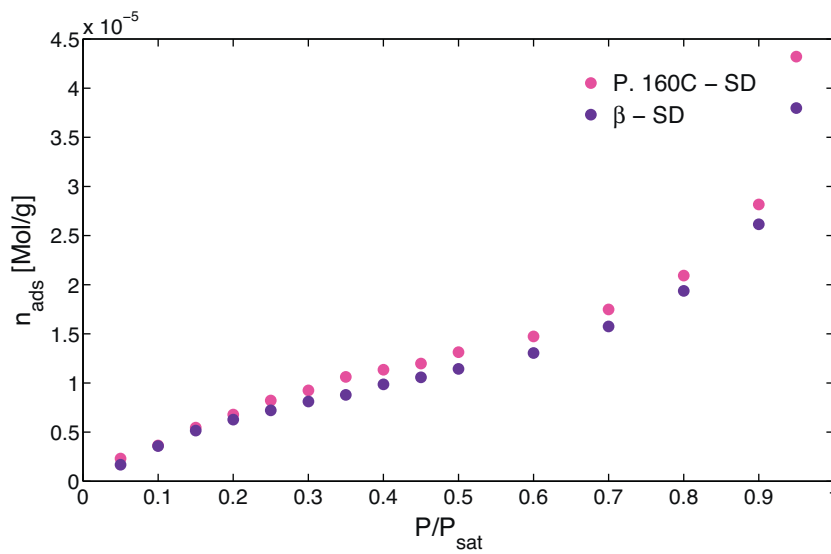


Fig. 7. Adsorption isotherms of  $\beta$ -SD and P160C-SD obtained by DVS using *n*-nonane as vapour probe.

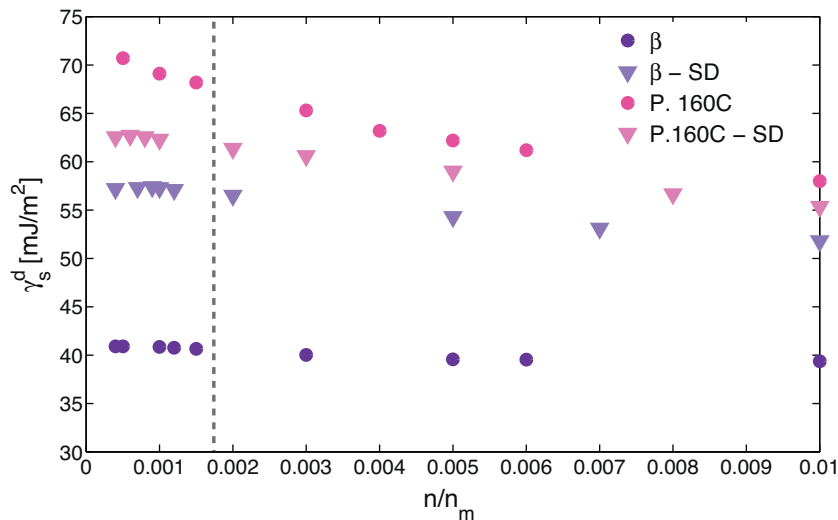


Fig. 8. Surface heterogeneity analysis of  $\beta$  mannitol samples, before and after spray drying.

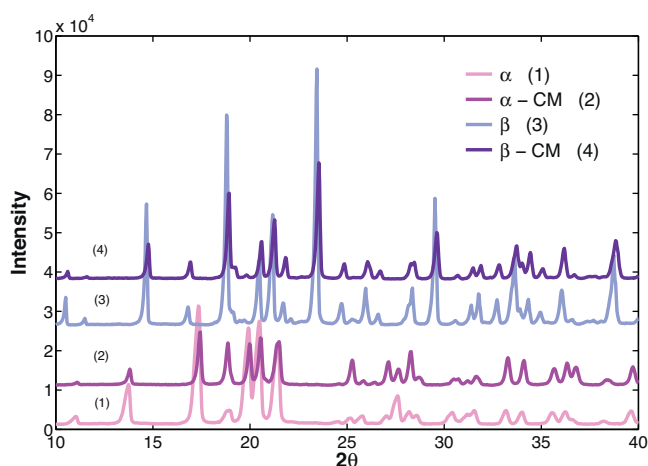


Fig. 9. X-ray patterns of  $\alpha$  and  $\beta$  mannitol samples before and after cryomilling.

samples are bigger than those of the  $\beta$  pure form but smaller than those obtained for the commercial powder P160C (Fig. 7). This tendency of the samples to have similar adsorption behavior after spray drying can be explained by the evolution of the particles to the same size and crystals habit. It seems important to highlight that the  $\gamma_s^d$  of P160C-SD is approximately  $5 \text{ mJ m}^{-2}$  bigger than the one of  $\beta$ -SD for all surface coverage studied ( $0.0004 < n/n_m < 0.01$ ). This difference, superior to the experimental error ( $< 1.3 \text{ mJ m}^{-2}$ ), can be attributed to the sorbitol presence in the commercial powder P160C, which one is conserved after spray drying the sample. It appears that small quantities of sorbitol in the powders (less than 1%) increase the strength of dispersive interactions of the solid dispersion.

After spray drying the samples we can found a region where the retention time does not depend on the injection volume (Fig. 8, dotted line  $n/n_m < 0.02$ ).

### 3.3. Cryogenic milled samples (CM)

The  $\alpha$  and  $\beta$  D-mannitol polymorphs generated by successive precipitation protocols were cryogenic milled in order to change its size and habit structure without changing their solid-state form. The abbreviations  $\beta$ -CM and  $\alpha$ -CM are used in this manuscript to identify the cryomilled powders.

#### 3.3.1. Powder crystallinity and purity

XRPD patterns were used to confirm polymorphism and to ensure the physical form of the samples.  $\alpha$  mannitol has characteristic reflection peaks at  $2\theta$  positions of  $13.7^\circ$ ,  $17.3^\circ$  and  $19.9^\circ$ , while for  $\beta$  mannitol are located at  $14.7^\circ$ ,  $18.8^\circ$  and  $23.6^\circ$ . As shown in Fig. 8, both  $\alpha$  and  $\beta$  pure samples keep their polymorphic form after cryomilling. Particle habit and size changes after CM can be depicted as a decrease of the characteristic peaks intensity.

#### 3.3.2. Particles size and habit by scanning electron microscopy (SEM)

SEM micrographs of the CM samples are shown in Figs. 10 and 11. The  $\alpha$ -CM samples are formed by agglomerates of approximately  $50 \mu\text{m}$  composed by small needle-like particles, and also by agglomerates of bigger particles always in needle-like shape as illustrated in Fig. 9. The closer zooms show that for  $\alpha$ -CM samples the direction of the fracture follows particles geometry. In fact, it seems that crystals fracture follows a plane perpendicular to the longitudinal axis of the needle.

The SEM analysis of the  $\beta$ -CM samples showed particles agglomerations. The powder seems to be composed by quite irregular particles habits between some micrometers and  $80 \mu\text{m}$ . A large quantity of small particles seems to be stick around the bigger ones. For this polymorph the fracture behavior after cryogenic milling is more complex and the solid seems to have a more brittle behavior (Fig. 11).

The results obtained by image analysis using the PVS830 showed for the  $\beta$ -CM a  $D[v, 0.1]$  of  $8 \mu\text{m}$ ,  $D[v, 0.5]$  of  $16 \mu\text{m}$  and  $D[v, 0.1]$  of  $30 \mu\text{m}$  while for the  $\alpha$ -CM samples a  $D[v, 0.1]$  of  $9 \mu\text{m}$ ,  $D[v, 0.5]$  of  $24 \mu\text{m}$  and  $D[v, 0.1]$  of  $40 \mu\text{m}$  were obtained. No real

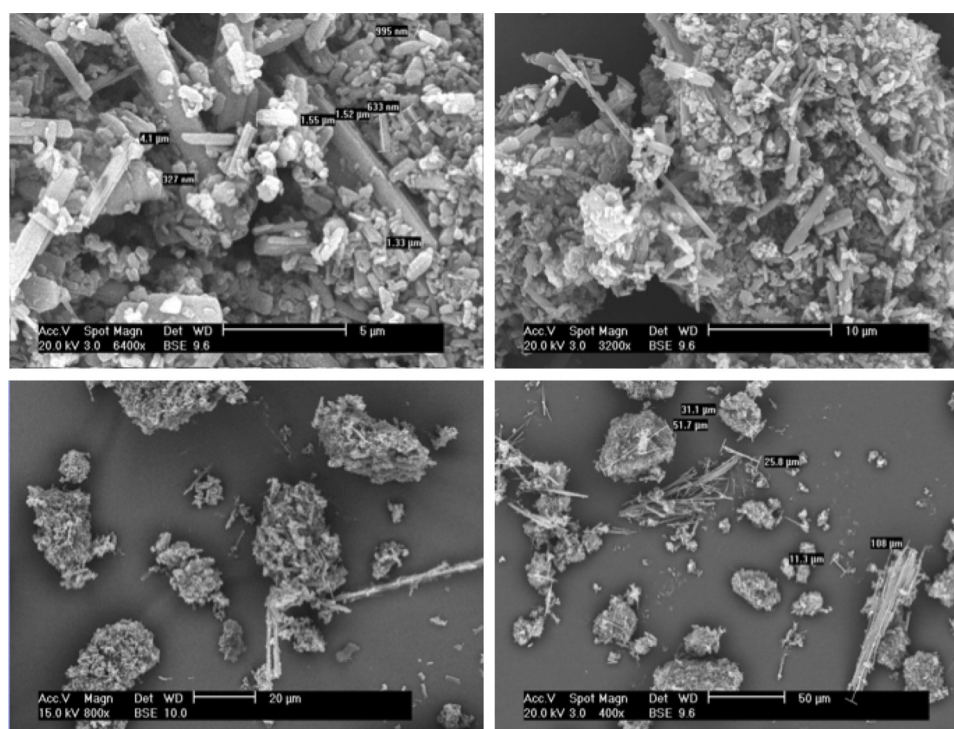


Fig. 10. SEM micrographs of  $\alpha$  mannitol cryomilled samples.

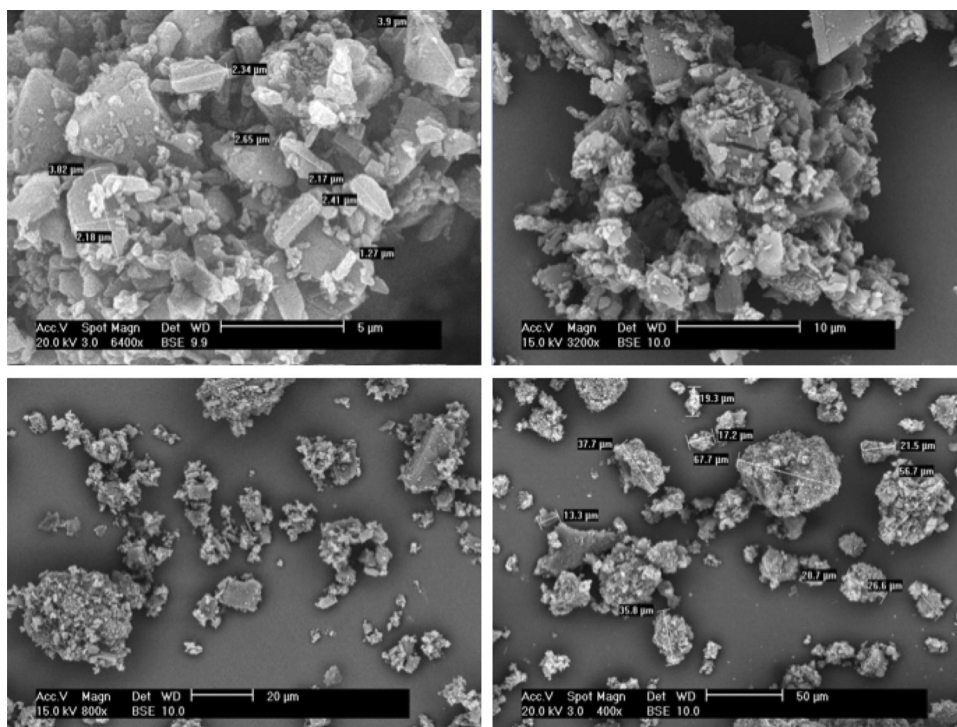


Fig. 11. SEM micrographs of  $\beta$  mannitol cryomilled samples.

differences were detected between the samples using this technique. The image analysis by SEM and by PVS830 differs, most of all due to particles agglomeration.

### 3.3.3. Surface energy analysis

After cryogenic milling both samples,  $\beta$ -CM and  $\alpha$ -CM, increased their specific surface areas. This increment allowed to analyze by DVS the  $\beta$ -CM samples thanks to an increment of the mass up-take at really low partial pressures, revealing a type II adsorption behavior (Fig. 12). This point is quite important, indeed if solid/probe molecules interaction showed a type III isotherm, probe-probe molecules interactions will be stronger than probe-

solid interactions and so the retention time measure by IGC will not be representative of the adsorption phenomenon.

Due to the low amount of experimental data (adsorbed amount as function of  $P/P_{\text{sat}}$  ranged between 0 and  $\sim 0.2$ ), between 3 and 4, and the low correlation coefficients obtained with the DVS data, the specific surface area calculations have been carried out using IGC.

As shown in Table 3, an increase in the dispersive surface energy of  $\beta$  and  $\alpha$  cryogenic milled samples, at low surface coverage, has been observed. Nevertheless, for the  $\alpha$ -CM sample this difference, with the  $\alpha$  pure sample, tends to decrease rapidly with increasing the injected amount. Indeed, for surface coverage superiors than 0.1% both solids,  $\alpha$  and  $\alpha$ -CM, have similar adsorption behavior.

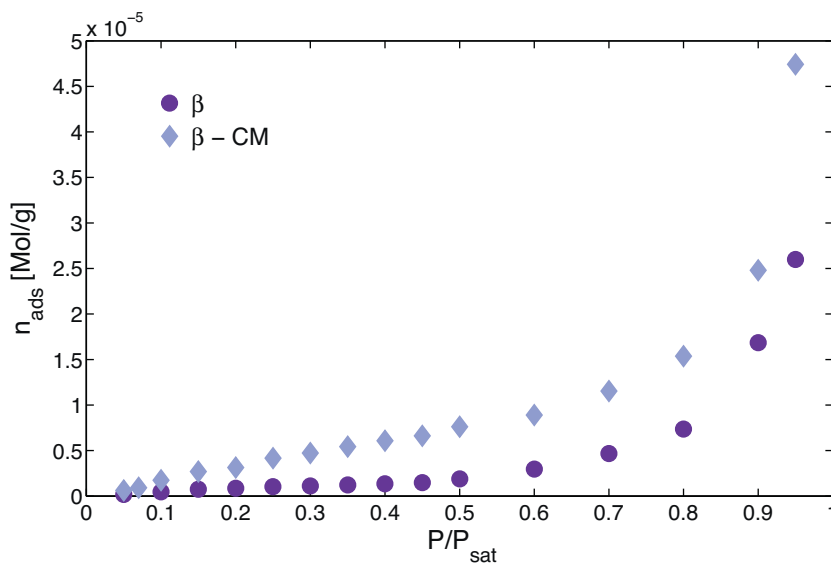


Fig. 12. Adsorption isotherms of  $\beta$  and  $\beta$ -CM obtained by DVS using  $n$ -nonane as vapour probe.

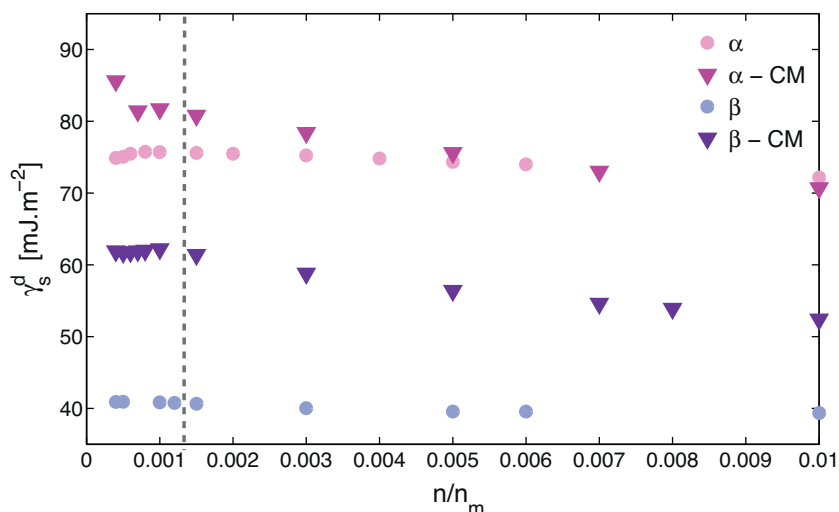


Fig. 13. Surface heterogeneity analysis of  $\alpha$  and  $\beta$  mannitol samples, before and after cryogenic milling (CM).

The  $\beta$ -CM sample has a similar but more energetic adsorption behavior than the  $\beta$  pure form. The region where  $\gamma_s^d$  does not depend on injection volume correspond to a ratio  $n/n_m$  lower than 0.002. Nevertheless, The  $\beta$ -CM sample is more heterogeneous, at low surface coverage, than the  $\beta$  pure sample. This more heterogenic adsorption behavior can be attributed to the anisotropic morphology of the  $\beta$ -CM particles (Fig. 13).

#### 4. Discussion

##### 4.1. Henry's domain determination by IGC

The first point to highlight is that after treatment, spray drying and cryogenic milling, the Henry's domain of each sample is reduced to really low surface coverage's ( $\theta_s < 1\%$ ). Thus, surface energy solid analyses do not allowed to represent the whole solids surface but allowed us to differentiate batches behavior.

It should be notice that the linearity of the isotherm, indicated by its correlation coefficient, plays a key role over the

determination of the maximum  $\theta_s$  that define Henry's domain, and should be well defined in this type of analysis. For example, for the  $\beta$ -SD samples, if we accept the linearity of the isotherm for  $R^2 > 0.99$ , a  $R^2 = 0.998$  corresponds to a  $P = 40$  Pa and so to a  $\theta_s = 10\%$  (Fig. 14a) while a  $R^2 = 0.999$  corresponds to a  $P = 140$  Pa and so to a  $\theta_s = 40\%$  (Fig. 14b). Nevertheless, we can see that even if  $R^2$  is higher taking account higher pressures, the data fit used does not represent quite well the first points. Thus, in this case, pressures smaller than 40 Pa are used to describe Henry's domain.

As  $\gamma_s^d$  is determinate by the injection of a series of alkanes  $n$ -octane,  $n$ -nonane and  $n$ -decane, Henry's domain will be determinate by the probe having the narrowest Henry's domain. As expected, the longer the chains of alkanes, the smaller the linear region of the adsorption isotherm. So in these experiences, the limit surface coverage to study surface energy by IGC in the infinite dilution region will be determined by the analysis of  $n$ -decane.

A high control of the injection size as an important number of experimental data points it is fundamental to determine with precision Henry's domain.

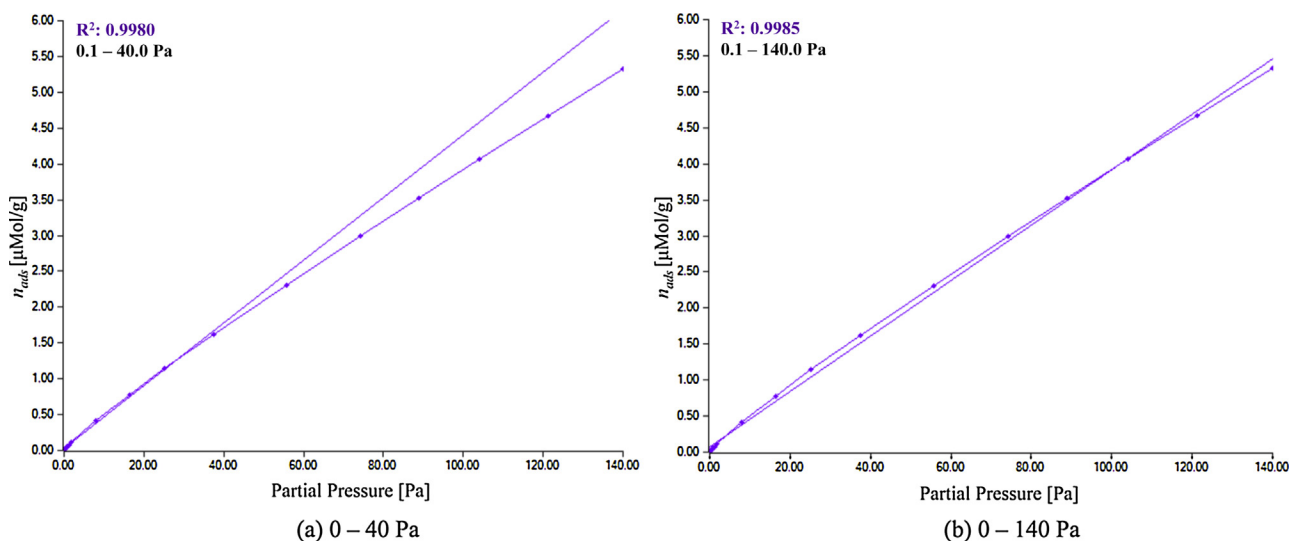
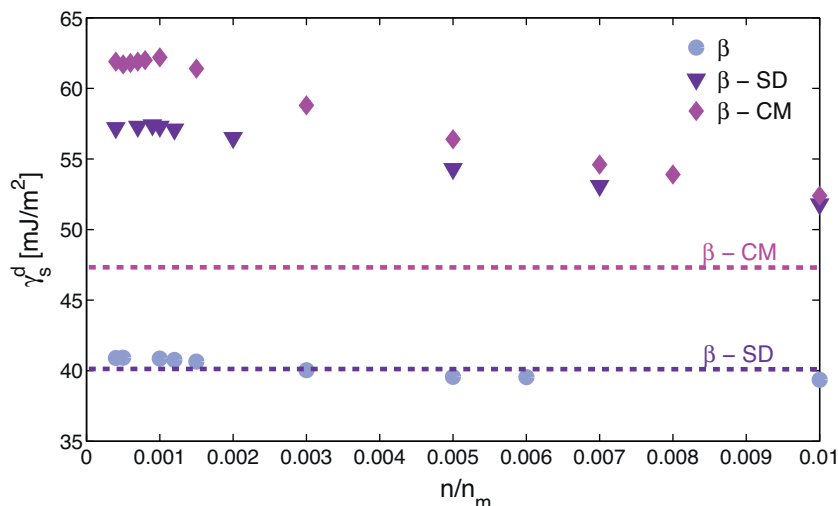


Fig. 14. Henry's domain determination by analysing the adsorption isotherms: example of  $\beta$ -SD/C<sub>9</sub>.



**Fig. 15.** Surface energy analysis by DVS (dotted line) and IGC of different pure  $\beta$  mannitol batches:  $\beta$  generated by antisolvent precipitation, after spray drying  $\beta$ -SD and after cryogenic milling  $\beta$ -CM.

#### 4.2. Dispersive surface energy

It is quite difficult to link crystal habit, size and agglomeration state to surface energy. Generally, surface energy differences after physical treatment such as milling, micronization, CM even SD amount others, are generally attributed to changes in particles size (surface area), morphology (habits), polymorphism (or amorphization) and to the exposure of more energetically active planes. During our experiences we took care to not change the solid state of the samples, thus no solid/solid transformations were obtained. Moreover it has been determined that for  $\beta$  mannitol, the most energetically active plane, in terms of dispersive surface energy, has a  $\gamma_s^d$  of  $44.1 \pm 0.6 \text{ mJ m}^{-2}$  (Ho et al., 2010). All this indicates that surface energy increments after CM and SD cannot be attributed to the exposure of new and more active phases or to solid-state transformations after treatment. Thus, crystal size and morphology changes seem to be responsible of surface energy increments in  $\beta$  mannitol samples. Nevertheless, we cannot separate particles size effect of crystals habit effect over the solid surface energy because CM and SD influence at the same time these two parameters.

As shown in Table 3, after cryogenic milling and spray drying treatment,  $\alpha$  and  $\beta$  mannitol samples presented an augmentation of its dispersive surface energy, at really low surface coverage. For the  $\beta$  form, three batches of different size and shape were generated. The first one obtained by antisolvent precipitation is composed by well defined sticks with smooth surfaces  $D[\nu, 0.5] = 26.7 \mu\text{m}$  and  $D[\nu, 0.9] = 81.7 \mu\text{m}$  (Fig. 3b). The  $\beta$ -SD sample is composed by well defined spheres between 1 and  $4 \mu\text{m}$  (Fig. 5a) while the batch  $\beta$ -CM is composed by agglomerations of quite irregular particles, of few micrometers to  $90 \mu\text{m}$ , with small particles stuck on the surface of the larger ones (Fig. 10).

IGC analysis revealed that these three batches have different surface behavior. After CM and SD the samples are more energetically active due to a change in the crystal habits. The  $\beta$ -recrystallized form appears as a quite homogeneous solid ( $\sim 40 \text{ mJ m}^{-2}$ ) while the  $\beta$ -CM batch and the  $\beta$ -SD batch showed a more heterogeneous surface, energetically speaking. It should be noted that despite its spherical shape and quite homogeneous size distribution,  $\beta$ -SD samples showed a slightly heterogeneous surface ( $57.3\text{--}51.7 \text{ mJ m}^{-2}$ ). This confirms that the particles surface is not as smooth as depicted by SEM analysis.

Surface energy analyses at really low surface coverage, allow us to differentiate the CM samples of the SD samples: for  $\beta$ -CM a  $\gamma_s^d$  of  $61.9 \text{ mJ m}^{-2}$  while for  $\beta$ -SD a  $\gamma_s^d$  of  $57.2 \text{ mJ m}^{-2}$  at  $\theta_s = 0.04\%$ . The  $\beta$ -CM particles are quite damaged and seem to have surface defects (Fig. 11). These surface irregularities can be seen as privileged sites where the probe molecules can be adsorbed by undergoing interactions from more than one surface. Surface energy analyses at really low surface coverage emphasize these differences. Indeed, if the injection volume is incremented,  $\theta_s > 0.1\%$ , the surface energy differences between  $\beta$ -CM and  $\beta$ -SD samples tend to disappear and both solids tend to similar adsorption behavior ( $\sim 52 \text{ mJ m}^{-2}$ ). Nevertheless, at this surface coverage both samples have a higher  $\gamma_s^d$  than the depart  $\beta$  form ( $52$  to  $40 \text{ mJ m}^{-2}$ , respectively). This difference can be still attributed to the influence of more energetically active sites related to size and crystal habit changes after SD and CM (Figs. 5 and 11).

It should be noted that if IGC-ID were defined for  $P/P_{\text{sat}} \sim 0.03$ , as most authors do it, we would worked outside Henry's domain and we would also mislead the effect of particles habits over solid's surface energy.

DVS analyses, which provided a mean value of the solid surface energy, showed that the  $\gamma_s^d$  of  $\beta$ -CM samples ( $47 \text{ mJ m}^{-2}$ , pink dotted line) is higher than the  $\gamma_s^d$  of  $\beta$ -SD samples ( $40 \text{ mJ m}^{-2}$ , purple dotted line). These results with surface energy analyses by IGC-ID show the contribution of more active sites to the solid average surface energy (Fig. 15). Moreover, IGC-DVS confrontation clearly shows us that if the more active sites are not numerous enough or not sufficiently higher than the most energetic active crystalline face, its influence can be misled by the techniques which provides a mean value of the solid surface energy like DVS. In fact, mean surface energy analyses can mislead to differentiate batches and thus mislead end-use properties.

For the  $\alpha$  form, two batches of different sizes were generated but with its morphology partially conserved. The  $\alpha$  mannitol generated by successive antisolvent precipitations is composed by needle-like particles of  $D[\nu, 0.5] = 25.3 \mu\text{m}$  et  $D[\nu, 0.9] = 42.4 \mu\text{m}$ . The  $\alpha$ -CM batch is formed by agglomerations of needle-like particles, between 20 and  $50 \mu\text{m}$ , but some non-agglomerated larger particles can also be found, always needle-like (Figs. 3 c and 10). Surface energy analysis showed a more energetically active  $\alpha$ -CM sample. Nevertheless, this is only true at low surface

coverage, indeed, for  $\theta_s < 0.005$  both samples showed a similar adsorption behavior (Fig. 15).

All these results can be better understood if the mathematical definition of the retention time is taken into account. In fact, as already highlighted in previous studies,  $t_N$  is the contribution of many interactions sites  $i$  and the interaction energy between the probe and the sites  $i$  (Cares et al., 2014). So, if the more active sites are not numerous enough its influence can be attenuated by the presence of less active ones, moreover, the influence of less active sites will be more important when increasing the injection size. The study of surface heterogeneity at higher surface coverage can give a more general idea of this point. Thus, for  $\alpha$ -CM samples, it seems that the more active sites created by this process are not numerous enough because the cryogenic milling of  $\alpha$  pure samples seems to only generate surface defects, which ones seem to be less active than the most energetically active face of the  $\alpha$  crystal.

Surface energy analysis by IGC at Henry's domain highlighted the influence of particles habits and size over solid's surface behavior. The combined set IGC and DVS validated this statement. Nevertheless, it is quite difficult to separate both effects because most processes affect at the same time solid's habits and size, even particles separation processes, such as sieving, are related to particles morphologies.

From a critical point of view, the study of surface energies in Henry's domain by IGC-ID, does not provide a global idea of the solid behavior. Indeed, SD and CM samples presented quite small linear adsorption region. Thus, only 1% of the surface can be "cover" to be in Henry's domain ( $\theta_s < 0.01$ ). So the question is, how far are we of the solid's "real" behavior; are we able to actually distinguish crystalline facets influence (surface chemistry), are those important? It seems necessary to have another technique of surface analysis such as DVS, or even molecular modeling. It will be also interesting to study surface heterogeneity by IGC using an equipment that allows a higher surface coverage and to use other mathematical models such as the energy distribution function.

## 5. Conclusions

Powder behavior depends directly of its interfacial interactions, thus of the physical and chemical characteristics of the particles of which it is composed. Nevertheless, it is difficult to link crystalline structure, habits, particles agglomeration state, size distribution and surface energy. Classically, surface energy increments after physical and mechanical treatment such as grinding, are attributed to changes in particles size (surface area), morphology (habits), solid state structure (polymorphism or amorphization) and/or to the exposure of more energetically active planes. In this work we studied the influence of particles habits and size distribution over the solid surface energy. To achieve this goal, two batches of pure  $\alpha$  and  $\beta$  mannitol, generated by successive crystallization protocols, were cryogenic milled and/or spray dried.

For the  $\beta$  form, three batches of different size and shape were studied. The first one, obtained by antisolvent precipitation, is composed by well defined sticks with smooth surfaces, the second one  $\beta$ -SD, is composed by well-defined spheres while the batch  $\beta$ -CM is formed by agglomerations of quite irregular particles. It is quite difficult to separate the effect of the size from the effect of particles habits because the two processes used, CM and SD, affected at the same time solid's habits and size. Moreover, even particles separation processes to study particles size, such as sieving, are related to particles morphologies.

IGC-ID studies highlighted surface energy differences between these three batches. Surface heterogeneity analyses, in Henry's domain ( $0.0004 < \theta_s < 0.01$ ), showed a quite heterogeneous and more energetically active  $\beta$ -CM ( $61.9$ – $52.4$   $\text{mJ m}^{-2}$ ) and  $\beta$ -SD ( $57.2$ – $51.7$   $\text{mJ m}^{-2}$ ) samples, and a quite homogeneous and less

active  $\beta$  form ( $\sim 40$   $\text{mJ m}^{-2}$ ). Surface energy analysis at low surface coverage,  $\theta_s < 0.01$ , allowed us to differentiate the SD samples of the CM samples. The solid size reduction, due to CM and SD, generates an increase of the specific surface area of the  $\beta$  pure powder, allowing DVS analysis of the  $\beta$ -CM ( $47$   $\text{mJ m}^{-2}$ ) and  $\beta$ -SD ( $40$   $\text{mJ m}^{-2}$ ) samples.

For the  $\alpha$  form, two batches of different size and a quite conserved needle-like morphology were studied. The first batch was generated by seeding and fast cooling while the second one,  $\alpha$ -CM, by the cryogenic milling of the first sample. Surface energy analysis at really low surface coverage,  $\theta_s < 0.005$ , showed a more energetically active  $\alpha$ -CM sample.

These results allow us to conclude that particles habits appear to be a major factor in the solid surface adsorption behavior of  $\text{D}$ -mannitol polymorphs. Moreover, it seems that there is a "threshold" above which the influence of more active sites, here attributed to surface irregularities, is attenuated and different batches of a same polymorph tend towards similar adsorption behavior. This threshold depends directly of the value of the more active sites but also of their number. If the more active sites are not numerous enough, or not sufficiently higher than the most energetic active face, its influence will be misled by the techniques which provides a mean value of the solid surface energy.

IGC-ID provides key information in terms of surface energy and appears to be a powerful tool to monitoring surface energy evolution as function of the generation process or after mechanical or thermal treatment. Even if the solid surface anisotropy is weak and maybe undetectable by standard analytical methods, it can make the solid more energetically active and thus more reactive. IGC-ID is able to detect weak surface energy variation, which may explain the behavior differences between batches, of a same polymorph, over time but also in atmospheres more or less moist.

## Acknowledgment

In the memory of Elisabeth Rodier (1966–2014).

## References

- Ahfat, N.M., Buckton, G., Burrows, R., Ticehurst, M.D., 2000. An exploration of inter-relationships between contact angle, inverse phase gas chromatography and triboelectric charging data. *Eur. J. Pharm. Sci.* 9 (3), 271–276.
- Brum, J., Burnett, D., 2011. Quantification of surface amorphous content using dispersive surface energy: the concept of effective amorphous surface area. *AAPS PharmSciTech* 12 (3), 887–892.
- Cares-Pacheco, M.-G., Vaca-Medina, G., Calvet, R., Espitalier, F., Letourneau, J.-J., Rouilly, A., Rodier, E., 2014. Physicochemical characterization of  $\text{D}$ -mannitol polymorphs: the challenging surface energy determination by inverse gas chromatography in the infinite dilution region. *Int. J. Pharm.* 475, 69–81.
- Chamarthy, S.P., Pinal, R., 2008. The nature of crystal disorder in milled pharmaceutical materials. *Colloids Surf. A: Physicochem. Eng. Aspects* 331 (1), 68–75.
- Crowley, K.J., Zografi, G., 2002. Cryogenic grinding of indomethacin polymorphs and solvates: assessment of amorphous phase formation and amorphous phase physical stability. *J. Pharm. Sci.* 91 (2), 492–507.
- Das, S., Larson, I., Young, P., Stewart, P., 2009. Surface energy changes and their relationship with the dispersibility of salmeterol xinafoate powders for inhalation after storage at high RH. *Eur. J. Pharm. Sci.* 38 (4), 347–354.
- Desprez, S., Descamps, M., 2006. Transformations of glassy indomethacin induced by ball-milling. *J. Non-Cryst. Solids* 352, 4480–4485.
- Feeley, J.C., York, P., Sumby, B.S., Dicks, H., 1998. Determination of surface properties and flow characteristics of salbutamol sulphate, before and after micronisation. *Int. J. Pharm.* 172 (1), 89–96.
- Feeley, J.C., York, P., Sumby, B.S., Dicks, H., 2002. Processing effects on the surface properties of  $\alpha$ -lactose monohydrate assessed by inverse gas chromatography (IGC). *J. Mater. Sci.* 37, 217–222.
- Feng, T., Pinal, R., Carvajal, M.T., 2008. Process induced disorder in crystalline materials: differentiating defective crystals from the amorphous form of griseofulvin. *J. Pharm. Sci.* 97 (8), 3207–3221.
- Gamble, J.F., Leane, M., Olusanmi, D., Tobby, M., Šupuk, E., Khoo, J., Naderi, M., 2012. Surface energy analysis as a tool to probe the surface energy characteristics of micronized materials: a comparison with inverse gas chromatography. *Int. J. Pharm.* 422 (1), 238–244.

- Hasegawa, S., Ke, P., Buckton, G., 2009. Determination of the structural relaxation at the surface of amorphous solid dispersion using inverse gas chromatography. *J. Pharm. Sci.* 98 (6), 2133–2139.
- Heng, J.Y., Thielmann, F., Williams, D., 2006. The effects of milling on the surface properties of form I paracetamol crystals. *Pharm. Res.* 8, 1918–1927.
- Ho, R., Hinder, S., Watts, J., Dilworth, S., Williams, D., Heng, J., 2010. Determination of surface heterogeneity of D-mannitol by sessile drop contact angle and finite concentration inverse gas chromatography. *Int. J. Pharm.* 387, 79–86.
- Ho, R., Naderi, M., Heng, J., Williams, D., Thielmann, F., Bouza, P., Keith, A.R., Thiele, G., Burnett, D., 2012. Effect of milling on particle shape and surface heterogeneity of needle-shaped crystals. *Pharm. Res.* 29, 2806–2816.
- Imaizumi, H., Nambu, N., Nagai, T., 1980. Stability and several physical properties of amorphous and crystalline forms of indomethacin. *Chem. Pharm. Bull. (Tokyo)* 28 (9), 2565–2569.
- Jones, M.D., Young, P., Traini, D., 2012. The use of inverse gas chromatography for the study of lactose and pharmaceutical materials used in dry powder inhalers. *Adv. Drug Deliv. Rev.* 64 (3), 285–293.
- Lee, Y.Y., Wu, J.X., Yang, M., Young, P.M., van den Berg, F., Rantanen, J., 2011. e of polymorphism in spray-dried mannitol. *Eur. J. Pharm. Sci.* 44 (1), 41–48.
- Lim, R.T.Y., Ng, W.K., Widjaja, E., Tan, R.B.H., 2013. Comparison of the physical stability and physicochemical properties of amorphous indomethacin prepared by co-milling and supercritical anti-solvent co-precipitation. *J. Supercrit. Fluids* 79, 186–201.
- Luner, P.E., Zhang, Y., Abramov, Y.A., Carvajal, M.T., 2012. Evaluation of milling method on the surface energetics of molecular crystals using inverse gas chromatography. *Cryst. Growth Des.* 12 (11), 5271–5282.
- Maas, S.G., Schaldach, G., Littringer, E.M., Mescher, A., Griesser, U.J., Braun, D.E., Urbanetz, N.A., 2011. The impact of spray drying outlet temperature on the particle morphology of mannitol. *Powder Technol.* 213 (1), 27–35.
- Nezzal, A., Aerts, L., Verspaille, M., Henderickx, G., Rendl, A., 2009. Polymorphism of sorbitol. *J. Crystal Growth* 311, 3863–3870.
- Newell, H., Buckton, G., 2004. Inverse gas chromatography: investigating whether the technique preferentially probes high energy sites for mixtures of crystalline and amorphous lactose. *Pharm. Res.* 21 (8), 1440–1444.
- Ohta, M., Buckton, G., 2004. Determination of the changes in surface energetics of cefditoren pivoxil as a consequence of processing induced disorder and equilibration to different relative humidities. *Int. J. Pharm.* 269 (1), 81–88.
- Otte, A., Carvajal, M.T., 2011. Assessment of milling-induced disorder of two pharmaceutical compounds. *J. Pharm. Sci.* 100 (5), 1793–1804.
- Otte, A., Zhang, Y., Carvajal, M.T., Pinal, R., 2012. Milling induces disorder in crystalline griseofulvin and order in its amorphous counterpart. *CrystEngComm* 14 (7), 2560–2570.
- Pilcer, G., Wauthoz, N., Amighi, K., 2012. Lactose characteristics and the generation of the aerosol. *Adv. Drug Deliv. Rev.* 64 (3), 233–256.
- Planinsek, O., Zadnik, J., Kunaver, M., Srcic, S., Godec, A., 2010. Structural evolution of indomethacin particles upon milling: time-resolved quantification and localization of disordered structure studied by IGC and DSC. *J. Pharm. Sci.* 99 (4), 1968–1981.
- Saxena, A., Kendrick, J., Grimsey, I., Mackint, L., 2007. Application of molecular modelling to determine the surface energy of mannitol. *Int. J. Pharm.* 343, 173–180.
- Shariare, M.H., De Matas, M., York, P., Shao, Q., 2011. The impact of material attributes and process parameters on the micronisation of lactose monohydrate. *Int. J. Pharm.* 408 (1), 58–66.
- Surana, R., Randall, L., Pyne, A., Vemuri, N.M., Suryanarayanan, R., 2003. Determination of glass transition temperature and in situ study of the plasticizing effect of water by inverse gas chromatography. *Pharm. Res.* 20 (10), 1647–1654.
- Tang, P., Chan, H., Choiou, H., Ogawa, K., Jones, M.D., Adi, H., Buckton, G., 2009. Characterisation and aerosolisation of mannitol particles produced via confined liquid impinging jets. *Int. J. Pharm.* 367, 51–57.
- Traini, D., Young, P.M., Thielmann, F., Acharya, M., 2008. The influence of lactose pseudopolymorphic form on salbutamol sulfate–lactose interactions in DPI formulations. *Drug Dev. Ind. Pharm.* 34 (9), 992–1001.
- Ticehurst, M.D., Rowe, R.C., York, P., 1994. Determination of the surface properties of two batches of salbutamol sulphate by inverse gas chromatography. *Int. J. Pharm.* 111 (3), 241–249.
- Thielmann, F., Burnett, D.J., Heng, J.Y., 2007. Determination of the surface energy distributions of different processed lactose. *Drug Dev. Ind. Pharm.* 33 (11), 1240–1253.
- Tong, H.H., Shekunov, B.Y., York, P., Chow, A.H., 2001. Characterization of two polymorphs of salmeterol xinafoate crystallized from supercritical fluids. *Pharm. Res.* 18 (6), 852–858.
- Tong, H.H., Shekunov, B.Y., York, P., Chow, A.H., 2006. Predicting the aerosol performance of dry powder inhalation formulations by interparticulate interaction analysis using inverse gas chromatography. *J. Pharm. Sci.* 95 (1), 228–233.
- Trowbridge, L., Grimsey, I., York, P., 1998. Influence of milling on the surface properties of acetaminophen. *Pharm. Sci.* 1, 310.
- Yamauchi, M., Lee, E.-H., Otte, A., Byrn, S.R., Carvajal, M.-T., 2011. Contrasting the surface and bulk properties of anhydrate and dehydrated hydrate materials. *Cryst. Growth Des.* 11 (3), 692–698.
- York, P., Ticehurst, M.D., Osborn, J.C., Roberts, R.J., Rowe, R.C., 1998. Characterisation of the surface energetics of milled D<sub>1</sub>-propranolol hydrochloride using inverse gas chromatography and molecular modelling. *Int. J. Pharm.* 174 (1), 179–186.